2015

Size-dependent chemical reactivity of silicon nanocrystals with water and oxygen

Melanie L. Mastronardi
University of Toronto

Kenneth K. Chen
University of Toronto

Kristine Liao
University of Toronto

Gilberto Casillas
University of Wollongong, gilberto@uow.edu.au

Geoffrey A. Ozin
University of Toronto

Size-dependent chemical reactivity of silicon nanocrystals with water and oxygen

Abstract

A detailed investigation examines how the size of allylbenzene-capped silicon nanocrystals (ncSi:AB) affects their chemical reactivity with gaseous O_2, H_2O, and O_2/H_2O as probed by in situ luminescence spectroscopy. Specifically, changes in the photoluminescence (PL) of size-separated ncSi:AB are monitored through alterations of their PL absolute quantum yield (AQY) as well as the wavelength and intensity of their PL spectra over time. These experiments, conducted under both continuous and intermittent illumination, help elucidate the roles of O_2, H_2O, and mixtures of O_2/H_2O, with respect to oxidation of ncSi:AB as a function of their size, providing vital information for any perceived application in advanced materials and biomedical devices.

Keywords

dependent, chemical, size, reactivity, oxygen, silicon, nanocrystals, water

Disciplines

Engineering | Physical Sciences and Mathematics

Size-Dependent Chemical Reactivity of Silicon Nanocrystals

Melanie L. Mastronardi,[†] Kenneth K. Chen,[†] Kristine Liao,[†] Gilberto Casillas,[α] Geoffrey A. Ozin[†*]

[†]Department of Chemistry, University of Toronto, 80 St. George Street, Toronto, Ontario, Canada, M5S 3H6

[α]UOW Electron Microscopy Centre, University of Wollongong, New South Wales 2500, Australia

ABSTRACT: The effects of exposure to dry and controlled humidity oxygenated atmospheres in the dark and light were examined in situ for monodisperse allylbenzene-capped silicon nanocrystals (ncSi:AB). Changes in photoluminescence (PL) intensity as measured by alterations of the PL absolute quantum yields (AQY) and blue shifting of PL spectra were measured over time under continuous and intermittent illumination to help elucidate the roles of O_2 and H_2O as well as UV irradiation in the oxidation of the ncSi surface. Size-dependent trends were observed for both PL blue shifting and changes in the PL AQY indicating that nanocrystal size plays an important role in how oxygen species react at the nanocrystal surface.

Introduction

Silicon nanocrystals (ncSi) were found to exhibit intense room temperature photoluminescence in 1990,[1] and subsequent study has identified that they possess size-dependant optical and electronic properties,[2a-c] similar to other semiconductor nanocrystals composed of heavy metal materials. In particular, quantum and spatial confinement effects result in a widening of the electronic band gap and a blue shift in photoluminescence (PL) as the ncSi particle size decreases.[2a-c,3] Recent studies also report that ncSi show size-dependent PL absolute quantum yields (AQY).[2a,c,4a,b] These size-dependent properties as well as a wide PL range that spans the visible to near infrared region,[2c] have established ncSi as a promising candidate in optoelectronic and biological imaging applications.[5a-e]

Currently, there are a variety of methods that exist for the synthesis of ncSi, including the annealing of SiO_x powders followed by etching with HF,[6] plasma synthesis,[7] and solution reduction of $SiCl_4$.[8] Colloidal stability of ncSi is easily achieved through a hydrosilylation reaction between surface Si-H groups and terminal alkenes.[9a-c] It is well established that surface capping with organic ligands helps to prevent unwanted oxidation of the nanocrystal surface;[9a,10] however, overtime even capped ncSi have been shown to oxidize under ambient conditions. Exposure to air overtime, resulting in surface oxidation, is known to quench the PL of ncSi as well as blue shift its emission wavelength.[4b,11] The blue shifting of PL has been attributed to the shrinking of the nanocrystalline core due from the formation of an oxide layer.[3,12] The formation of dangling bonds and defect sites in the oxide layer create surface states in the band gap that effectively quench the PL.[13a,b]

To date little is known regarding the role O_2 and H_2O plays in oxidation processes for ligand capped ncSi, but there are a variety of reports outlining different processes through which unfunctionalized or hydride-capped ncSi interact with H_2O and O_2.[13a,14a-c] Investigation of the oxidation of ncSi:H nanocrystals by electron spin resonance was reported to be consistent with the Cabrera-Mott theory of oxidation in ambient-air.[13a] The process is proposed to involve an induction period where the preferential adsorption of H_2O near surface silanol (Si-OH) groups aids the cleavage of an adjacent Si-Si bond, which transfers an electron to an adsorbed O_2 and attracts it to the cleaved bond. Reaction of the O_2 at this site then leads to the formation of two Si-O-Si groups. Studies of bulk-Si surfaces indicated that the duration of the induction period is inversely proportional to humidity and density of Si−OH groups.[15a,b]

Hydride-terminated ncSi (ncSi:H) have been shown to be efficient photosensitizers of singlet oxygen due to their highly developed surfaces and long radiative lifetimes.[14a,b] This process quenches the PL of ncSi as energy is transferred from optically excited excitons to O_2 molecules adsorbed on the ncSi surface and is most efficient at a PL wavelength of 760nm (1.63 eV), which corresponds to the energy transition energy from the O_2 triplet state to excited singlet state.[14b] PL quenching has been shown to be a reversible effect provided that the ncSi:H have not been exposed to O_2 under prolonged illumination, which leads to an irreversible photooxidation process that degrades the PL permanently.[14c] Singlet O_2 energy is not enough to break a Si-Si bond, therefore thermal energy is also required for the formation of Si-O-Si, which has been reported to form quicker at higher temperatures.[14c]

While oxide formation at the ncSi surface tends to result in PL quenching, in some cases PL enhancement has

also been observed; this is attributed to oxidation-induced passivation of dangling bonds.[3,16a,b] It has been proposed that the apparent discrepancy between different studies may result from variations in initial surface passivation and oxidation conditions.[13a] Overall the consensus is that interfacial defects and Si dangling bonds strongly influence the optoelectronic properties of ncSi,[13a] which means that understanding the surface structure of ncSi and how it oxidizes is of utmost importance for developing functional ncSi materials, particularly for colloidally-stable ligand-capped ncSi of varying size.

In order to probe the effects of oxidation on different sizes of organic capped ncSi, we report the results of chemical reactivity studies performed on allybenzene-capped ncSi that have been size-separated into relatively monodisperse fractions using size-selective precipitation.[2a]

Experimental

Reagents and Materials. Trichlorosilane (HSiCl3, 99%) was purchased from Sigma Aldrich, stored in a refrigerator, and used as received. Hydrofluoric acid (ACS reagent 48%, Sigma Aldrich), ethanol (anhydrous, Commercial Alcohols), methanol (ACS reagent, Sigma Aldrich), toluene (anhydrous, Sigma Aldrich), isopropanol (ACS, EMD), potassium hydroxide (technical grade, ACF), hexanes (ACS reagent, Caledon Laboratories), and phenyltriethoxysilane (98%, Aldrich) were used as received. Allylbenzene (98%, Aldrich) was filtered through activated neutral alumina (type WN-3, Sigma Aldrich) and a 0.2 μm PTFE syringe filter before use to remove any peroxide impurities.[17] Argon compressed gas (ultra-high purity, Praxair) and 49.9% oxygen balance argon compressed gas (certified standard, Praxair) were purged through deionized water or Drierite.

Synthesis of Size-Separated ncSi:AB. Size-separated allylbenzene-capped ncSi were synthesized using a previously reported method with some modifications.[2a] This method involves the high temperature thermal processing of sol-gel hydridosilicate (HSiO$_{1.5}$) glasses derived from trichlorosilane (HSiCl$_3$), followed by etching with HF to liberate the ncSi from the encapsulating SiO$_2$ matrix. The hydride-terminated ncSi were functionalized with allylbenzene groups using a thermally-initiated hydrosilylation reaction in neat allylbenzene to produce a stable, concentrated colloidal dispersion. The ncSi that were too large to be stabilized with allylbenzene caps were removed from the reaction mixture by centrifugation and the ncSi:AB were isolated from the excess un-reacted allylbenzene by vacuum distillation followed by heating under vacuum at 155°C for 5.5 hours to removed excess alkenes.[18] The purified polydisperse ncSi:AB were re-dispersed in toluene, resulting in a clear orange solution that displayed bright orange-red photoluminescence (PL) under photoexcitation (λ_{exc} = 365 nm). Size-selective precipitation was performed on the toluene dispersion of polydisperse ncSi:AB, using methanol as the anti-solvent to isolate fractions of relatively monodisperse ncSi:AB. Following each addition of methanol, the cloudy solution was briefly sonicated then centrifuged for 10 mins at 6461 rpm. The clear supernatant was decanted and the solid was immediately redispersed in toluene. In order to ensure sample purity, each fraction was precipitated a second time. Immediately after the supernatant was decanted after the second precipitation the solid precipitate was transferred into a glove box in order to minimize surface oxidation from exposure to air. In the glove box, the solid precipitate for each fraction was dispersed in anhydrous toluene and stored until used.

Preparation of ncSi:AB Films. Glass slide substrates were treated in a mixture of KOH and isopropanol (sonicated for one hour and left overnight), then rinsed with distilled water and dried in an oven. Dried substrates were then coated with phenyltriethoxysilane and heated in an oven at around 120°C for 3 days. The substrates were then rinsed with hexanes, dried and transferred to a glove box. 40ul of a toluene dispersion of ncSi:AB was then drop-coated onto the hydrophobic glass substrates, and allowed to dry.

Characterization. Scanning transmission electron microscopy (STEM) images were acquired in a probe-corrected JEOL ARM200F operated at 80 kV equipped with a cold field emission gun and a high resolution pole-piece. Middle angle annular dark field (MAADF) images were acquired with 45 and 180 mrad inner and outer collection angles respectively, while bright field images used 11 mrad collection angles. Both images were recorded with a dwell time of 38 μs, and convergence semi-angle of 25 mrad resulting in a probe current of 40 pA. Samples were drop-cast onto Graphene-Cu grids (Graphene Supermarket) to ensure an ultra-thin support film of less than 2 nm. At least 500 particles were measured by hand to determine the average particle diameter and standard deviation values of the ncSi:AB from microscopy images. The photoluminescence of the ncSi:AB fractions was obtained using the absolute quantum yield set-up described below. The absolute quantum yield was determined using a previously reported integrating sphere method.[19] Samples were excited in an integrating sphere (Gigahertz Optik, custom made) with light from a 365nm LED (Thorlabs M365L2), and photoluminescence was collected by a 1 mm diameter optical fibre (Ocean Optics) and detected by an Ocean Optics Maya 2000 spectrometer. The continuous absolute quantum yield was measured by taking appropriate ratios of the excitation and emission peak areas of spectra recorded for the empty sphere and sample holder, and the excitation focused directly onto the sample.[20] The accuracy of the system was verified against literature values for rhodamine 6G and MEH-PPV. Solution samples were measured in cuvettes that were filled and sealed in the glove box. Film samples were sealed into a custom made sample holder in the glove box that was then inserted into the integrating sphere. The continuous AQY of each film sample was measured over a period of 300 seconds (5 minutes), and intermitted illumination was achieved by blocking the LED light from hitting the sample over short periods of time throughout the 5 minute measurement. During each measurement, the film samples were exposed to different atmospheres. Dry argon and dry 50% oxygen in argon were created by flowing gas through a tube containing Drierite. Wet argon and wet 50% oxygen in argon were created by flowing gas through a bubbler filled with deionized water. The hu-

midity of the atmospheres was monitored using a relative humidity probe (RH-USB, Omega Engineering, Inc.). All AQY and PL film experiments were conducted in duplicate, and the extracted AQY and PL values were averaged wherever possible. PL spectra were smoothed and baseline corrected using Origin Pro 8 software. Fourier transform infrared (FTIR) spectroscopy was performed on a Perkin Elmer Spectrum One FTIR spectrometer and peak areas were determined using Spectrum software. For pristine samples, films of ncSi:AB were drop-cast onto an IR transparent KBr substrate in the glove box, covered with a second KBr substrate, and sealed with Teflon tape. For samples exposed to different atmospheres, films of ncSi:AB were drop-cast onto 6mm by 1mm KBr plates, loaded into the resealable continuous AQY sample holder in the glove box, and exposed to the gas flow as above, under illumination in the integrating sphere or in the dark. The plates were then removed and run immediately under ambient conditions. X-ray photoelectron spectra (XPS) were obtained using a Thermo Scientific Theta Probe utilizing monochromatic Al K α radiation, and spectra were calibrated to the C1s emission arising from adventitious hydrocarbons (284.8 eV). The high-resolution Si 2p region of the XPS was fit for the dominant Si species (Si^0, Si^{+1}, Si^{+2}, Si^{+3}, and Si^{+4}). The atomic % determined from the area of the C1s, O1s and $Si2p^0$ peaks were used to compare the extent of surface oxidation of pristine and air exposed samples of varying sizes.

Results and Discussion

The polydisperse ensemble and select size-separated ncSi:AB samples were characterized by scanning transmission electron microscopy (STEM). Particle size analysis confirms the expected decreasing particle size with increasing size-selective precipitation step (**SI Figure 1**). The average diameter values were measured as 2.79 ± 1.7 nm for the ensemble, 2.22 ± 0.5 nm for fraction 11, 2.14 ± 0.4 nm for fraction 13, 2.01 ± 0.4 nm for fraction 16, and 1.81 ± 0.4 nm for fraction 18. All fractions contain some degree of crystallinity, with crystal lattice lines appearing in the images of all samples examined. However, lattice fringes are not observed for all particles, which may be due to random orientation of the particles and beam damage that causes the particles to amorphise before an image can be acquired. It is not possible to say if all particles were crystalline to begin with, but there are certainly some crystalline particles observed for all fractions including fraction 18, which contains the smallest particles (**SI Figure 2**).
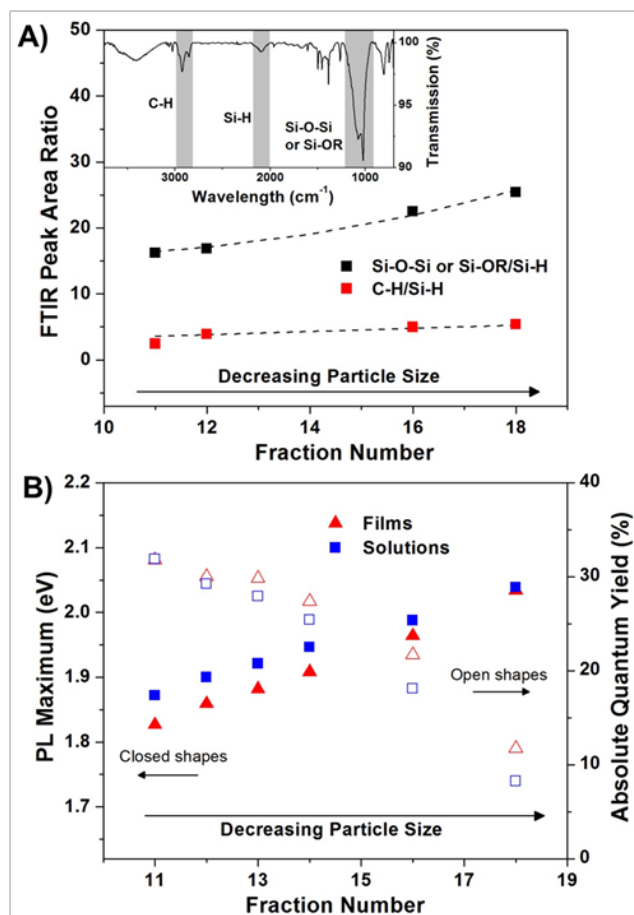

Figure 1. Characterization of Size-Separated ncSi:AB. A) Ratios of FTIR peak areas plotted for select size-separated ncSi:AB fractions. Inset, denotes peak area regions examined on the FTIR spectrum of fraction 11. **B)** Photoluminescence (PL) maximum and PL absolute quantum yield (AQY) plotted versus fraction number for both film and solution samples show the variation of values for each fraction in different forms. The difference in PL maximum value decreases while the difference in AQY increases with decreasing size.

Select pristine samples of size-separated ncSi:AB were analyzed using Fourier Transform infrared (FTIR) spectroscopy. The FTIR spectrum shown for fraction 11 (**Figure 1A, inset**) shows the characteristic stretching modes associated with allybenzene capped ncSi, consistent with previous work.[2a] To compare the surface species present for fractions of different size, ratios of the areas associated with Si-H, C-H, and Si-O-Si or Si-OR stretching modes are plotted in **Figure 1A**. The ratio of C-H to Si-H areas increases slightly with decreasing size, indicating that there is a higher proportion of allylbenzene ligands to Si-H species at the surface of smaller ncSi:AB. This can be explained by the increasing surface curvature of particles with decreasing size. Complete surface coverage of ncSi with any alkyl ligand is not possible due to the disparity between the diameter of an alkyl chain carbon (4.2 Å) and the spacing between silicon atoms on the Si surface (3.85 Å for 111).[21] Ligand cone models have been reported and used to estimate the surface coverage of ligands on nanoparticle surfaces.[22] For allylbenzene, which has a higher ligand cone angle compared to a linear alkyl group, a higher surface curvature

will allow more room for ligands to spread out from the nanocrystal surface, allowing more Si-H species to be converted to Si-AB with decreasing particle size. The presence of adventitious surface oxidation has been reported in previous syntheses of organic capped ncSi,[5c,23] and the results here show the ratio of the peak associated with Si-O-Si or Si-OR to Si-H increasing with decreasing size, indicating that a greater proportion of oxide species exist at the ncSi:AB surface of smaller particles. This size-dependent adventitious surface oxidation trend is also observed in comparing the atomic % of core Si, O and C species determined by XPS for particles of varying size (**SI Figure 3A**). The Si-H species that remain at the ncSi:AB surface likely react with residual oxygen dissolved in the toluene or methanol itself, which was used as the anti-solvent in the size-separation step. The size-dependence of the adventitious surface oxidation can be explained by the increasing spacing between the ligand tails that make it easier for oxide species to reach the surface with increasing curvature,[24] as well as the fact that smaller sized particles were exposed to methanol for longer time periods due to the nature of the size-separation process. Despite the presence of oxide surface species, there is still a significant peak associated with Si-H for all fractions, indicating the presence of sites with which oxygen species in the oxygen and water rich environments used can react for this chemical reactivity study.

The PL spectra and PL AQY were measured for select pristine fractions of ncSi:AB both dispersed in toluene and drop-coated onto treated hydrophobic glass slide substrates. The AQY shows a decreasing trend with decreasing particle size for both film and solution samples (**Figure 1B**), which is consistent with previous reports of similarly sized ncSi.[2a,4b] In previous work, the AQY decrease has been attributed to a decrease in ncSi core crystallinity with decreasing particle size, as well as an increase in the competing non-radiative relaxation surface trap and defect pathways that become more prevalent with decreasing ncSi size.[2a] The microscopy and FTIR results presented here tend to favor the later explanation, since some crystallinity is observed for even the smallest particles imaged and the ratio of oxide species, likely to contribute to surface traps and defect sites, is shown to increase with decreasing particle size.

Consistent with the effects of quantum confinement, the PL maximum blue shifts with decreasing particle size for both film and solution samples (**Figure 1B**).[4a,13b] A slight red shift in PL peak emission for film versus solutions samples is attributed to greater particle interactions in the solid state film samples, resulting in interparticle coupling or efficient energy transfer from the smaller particles to the larger particles.[25a,b]
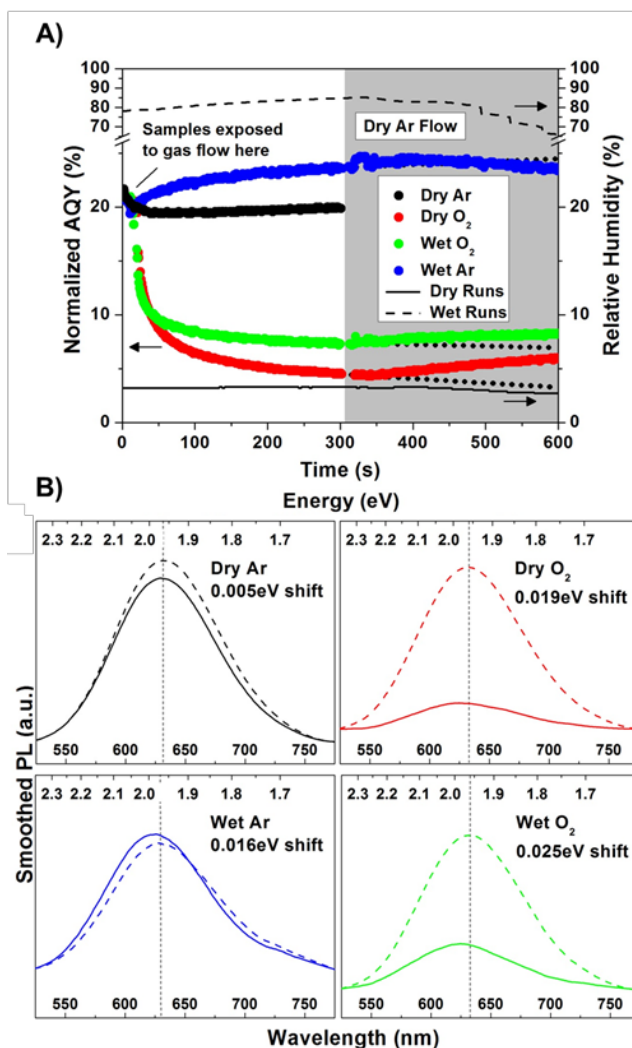
Figure 2. Continuous Absolute Quantum Yield Measurements. **A)** Photoluminescence (PL) absolute quantum yield (AQY) curves for fraction 16 measured under different atmospheres, showing representative relative humidity curves for dry and wet atmospheres. The AQY curves have been normalized to the average initial AQY value. After 300s the atmospheres containing H_2O and/or O_2 were purged for 300s with dry Ar flow through the system. The dotted lines shown following the switch to dry Ar are guides to help visualize the changes in AQY. **B)** PL spectra for fraction 16 measured before (dashed line) and after exposure (solid line) to each atmospheres for 300s. PL spectra have been smoothed for clarity. PL blue shift from the initial value for each atmosphere is denoted in eV.

In order to probe the effect different oxygen species have on the optical properties of ncSi:AB, the AQY was measured continuously while film samples of select fractions were exposed to different atmospheres. Initially each sample was prepared and sealed under nitrogen; the samples were then exposed to one of the following atmospheres: dry argon, wet argon, dry 50% oxygen in argon (referred to as dry O_2), and wet 50% oxygen in argon (referred to as wet O_2). PL spectra were measured initially and after exposure to each atmosphere for 300s. To help elucidate the extent of non-chemical quenching observed select films were subsequently purged with dry Ar following exposure to O_2 and H_2O containing atmospheres. The relative humidity was monitored during all

continuous AQY measurements using a relative humidity sensor. In addition to the continuous AQY measurements outlined above, film samples were run under all atmospheres with intermittent illumination to study the effect of light on the reactivity of H_2O and/or O_2 species at the ncSi:AB surface.

AQY curves and relative humidity curves representative of wet and dry conditions under continuous illumination are shown for fraction 16 in **Figure 2A** and the corresponding PL spectra are shown in **Figure 2B**. In the analysis of Figure 2, it is useful to assume a baseline with the results of inert dry Ar exposure at 300s where the signals have stabilized in order to measure and understand the effects of H_2O and O_2. Despite efforts to purge and eliminate air from the testing apparatus, it is likely that some residual ambient air remained; this is demonstrated by a slight decrease in AQY (from 22 to 20%) and slight blue shift in PL maximum (0.005eV) observed for the P16 dry Ar sample. Recent work suggest that exposure to UV light under inert conditions results in a decrease in AQY due to non-oxidative photobleaching,[26] which may also be contributing to the decrease in AQY we observe. However, the work presented here was performed on much a shorter timescale and in our case we observe a blue shift in PL indicating that oxidation from residual air is the dominant effect at play.

Upon exposure to atmospheres containing O_2 (both wet and dry) a significant decrease in AQY was observed. At 300s, AQY values were 7% and 4.5% for samples exposed to wet O_2 and dry O_2, respectively. Additionally, we see that the PL has blue-shifted for both dry (0.019eV) and wet O_2 (0.025eV). Since blue shifting of ncSi emission energy has been attributed to shrinking of the nanocrystalline core due to the formation of an oxide layer for ncSi exposed to air overtime, it can be inferred that some form of irreversible oxidation is occurring for samples in all atmospheres. This oxidation would also result in some PL quenching (decrease in AQY) due to the emergence of intermediate states caused by the formation of dangling bonds and defect sites.[13a,b] The large AQY decrease and PL blue shift observed for both samples exposed to O_2 indicate that surface oxidation is responsible for a large extent of the optoelectronic changes.

Purging with dry Ar beginning at 300s, results in an increase of the AQY of dry O_2 treated ncSi:AB from 4.5 to 6% and an increase from 7 to 8% for wet O_2 treated samples by 600s. Based on this increase in AQY we propose that the AQY decrease observed at 300s is due to a combination of defect states formed from irreversible surface oxidation as well as photosensitization, which would give some reversible PL quenching. Photosensitization in this case describes the process where photogenerated singlet oxygen molecules cause photodegradation in silicon.[14c] Molecular oxygen adsorbed to ncSi surfaces act as a competing mechanism through which photogenerated excitons within the ncSi may transfer its energy, leading to the generation of singlet oxygen. The reactive photogenerated singlet oxygen may then react with the ncSi surface, leading to irreversible photooxidation. It is likely that the dry Ar purge at 300s removed some of the adsorbed oxygen to reduce its depressing effect on the AQY.
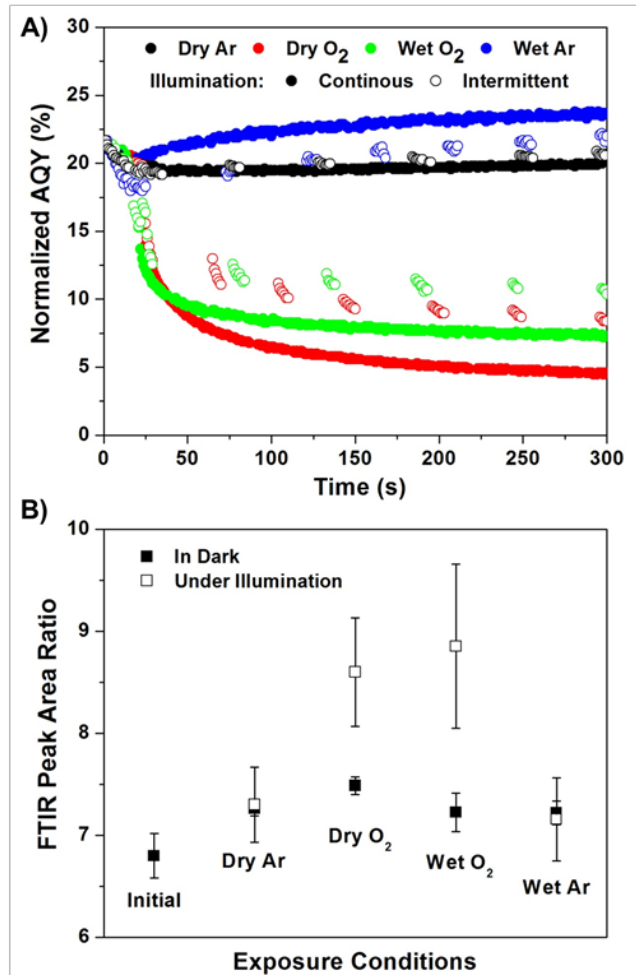
Figure 3. A) Absolute quantum yield (AQY) curves for fraction 16 measured under different atmospheres with continuous and intermittent illumination. **B)** Ratio of the Si-O-Si/Si-OR to Si-H peak areas for fraction 10 initially and after exposure to different conditions under illumination and in the dark for 300s.

The contribution of H_2O on irreversible surface oxidation and photosensitization is difficult to quantify, but by comparing the results of wet and dry O_2 exposure in **Figure 2**, we begin to see a few trends. The larger initial AQY decrease and lower AQY increase with dry Ar purging for wet O_2 compared to dry O_2 (**Figure 2A**), suggests that a greater extent of irreversible surface oxidation versus photosensitization is contributing to the AQY changes in the wet O_2 atmosphere. Additionally, we observe a larger blue shift for wet O_2 (0.025eV) compared to dry O_2 (0.019eV) (**Figure 2B**). These results are consistent with reports where H_2O passivates dangling bonds generated by oxidation by forming Si-OH groups,[13a] and higher humidity with higher density of Si-OH groups helps shorten the induction period for surface oxidation of Si.[15a,b]

In **Figure 2**, ncSi:AB exposed to wet Ar shows an increase in AQY up to 4% above the dry Ar baseline, with a PL blue shift (0.016eV) that is 3 times greater than that of ncSi:AB exposed dry Ar after 300s. The larger blue shift compared to dry Ar is likely the result of residual air in the system, as previously described, that in the presence of H_2O would be much more likely to oxidize the

surface. It has been proposed that physisorbed H_2O may be responsible for air-induced PL degradation of ncSi;[26] however, the results presented here indicate that this is not the case when ncSi:AB is exposed to pure H_2O. The increase in AQY is likely due to H_2O passivation of defects states and dangling bonds present on the ncSi:AB surface.[13a] With dry Ar purging after 300s, the AQY continues to increase slightly then begins to decline after about 450s. Assuming the interaction between ncSi:AB and pure H_2O to passivate defects takes place as both a chemical reaction and physical adsorption, removing some of the excess H_2O with dry Ar purging could result in reducing the passivation effect thereby decreasing the AQY.

Since a source of photogenerated excitons is a key to photosensitization of O_2 and subsequent photooxidation, an experiment with intermittent, rather than continuous illumination and AQY measurement was conducted as shown in **Figure 3A**. The results show that when intermittent illumination is used the overall effect of each atmosphere on the AQY is not as severe as with continuous illumination, indicating the strong role of light in the interaction between H_2O and O_2 with the ncSi:AB surface. At 300s exposure, despite the presence of some residual air, the AQY for ncSi:AB exposed to dry Ar remains stable at approximately 20.5%. Intermittent illumination results in minimizing the AQY decrease for ncSi:AB in dry O_2, reaching only about 8.5% instead of 4.5% under continuous illumination after 300s. In wet O_2 the ncSi:AB AQY decrease is minimized as well but to a slightly lower extent, reaching only about 10% instead of 7% under continuous illumination. The lower decreases observed for O_2 exposed samples are consistent with previously reported work of polydisperse ncSi exposed to air and with and without UV illumination.[26] The ncSi:AB exposed to wet Ar increases to about 22%, which is slightly lower than the value of 24% achieved under continuous illumination, indicating that the passivation of surface defects is promoted with additional energy.
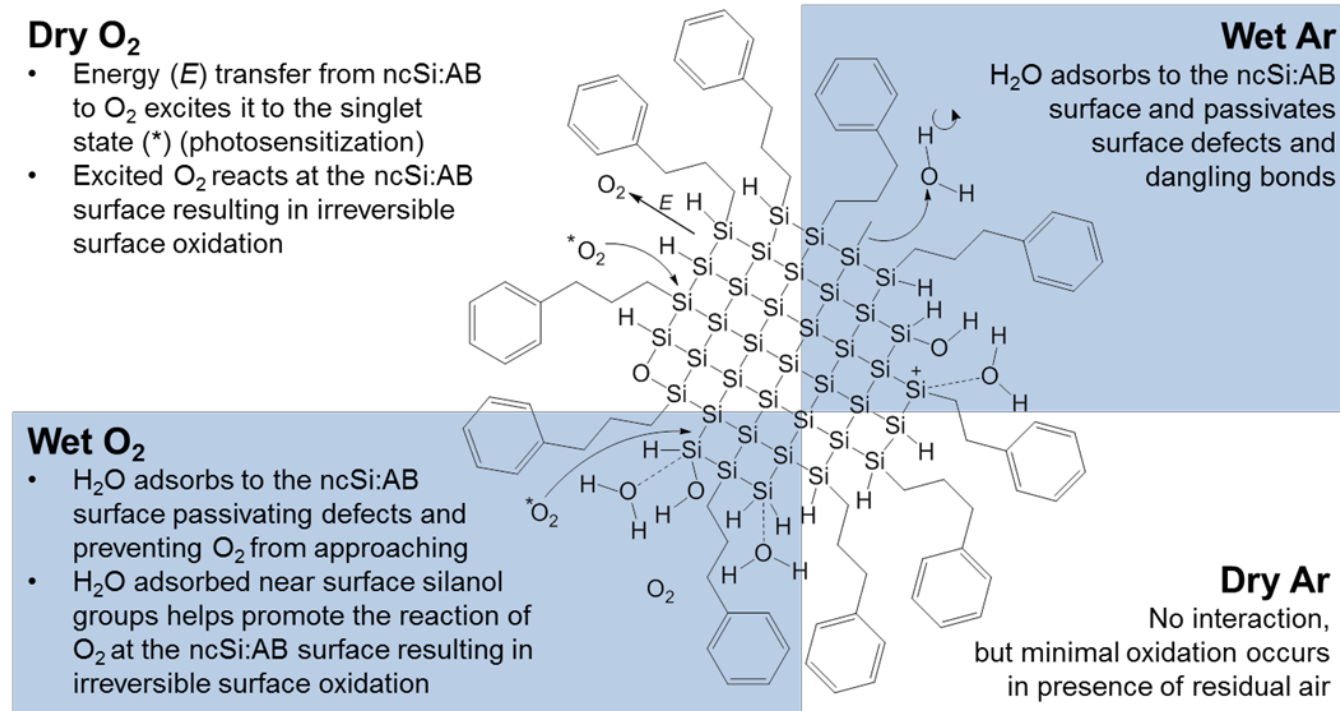
To confirm the effect of photosensitization on surface oxidation and ultimately the AQY and PL maximum, film samples of fraction 10 drop-coated on KBr windows were subject to the four atmospheres and FTIR measurement of the samples were taken. The area ratios of peaks assigned to Si-H stretch (2100 cm^{-1}) and Si-O-Si/Si-OR stretch (1090 cm^{-1}) were plotted in **Figure 3B**. Compared to the initial value, all samples show a slightly higher ratio due to oxidation attributed to residual air prior to the experiment. While there is almost no difference in the ratio for wet and dry Ar, both dry and wet O_2 exposed samples show a significantly higher ratio under continuous illumination, which is evidence of the extent photooxidation contributes to the formation of Si-O-Si species and the optoelectronic changes observed. Unfortunately, the extent of Si-OH on the ncSi:AB surface

cannot be probed using FTIR under wet and dry conditions as the Si-OH peak overlaps with the peak associated with adsorbed H_2O in the region between 3200-3600cm^{-1}.
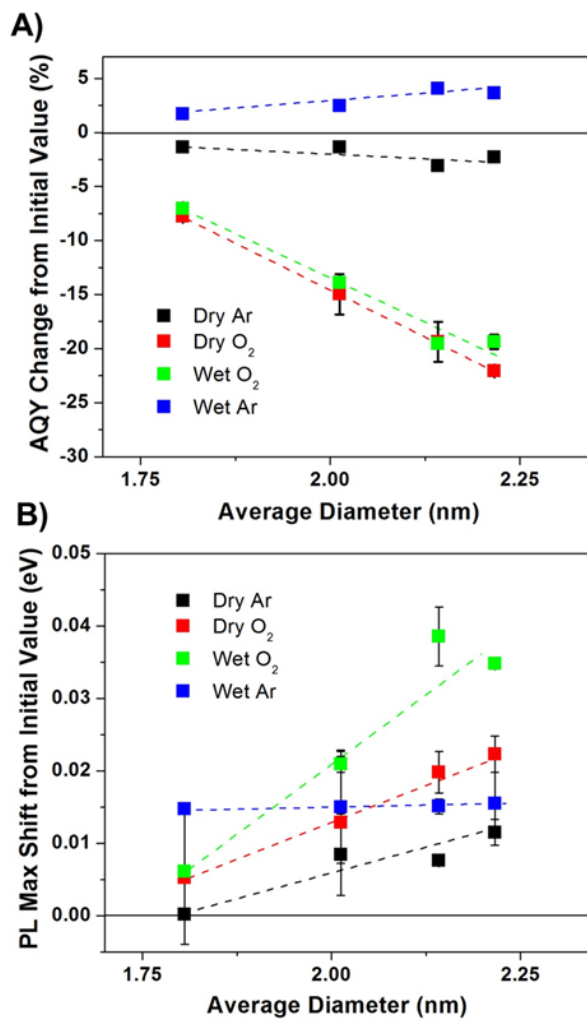
Figure 4. Size-Dependence of AQY and PL Maximum Shifts. A) The value by which the PL AQY changes after exposure to various atmospheres compared to its initial AQY is plotted for several different sized fractions. Dashed lines are shown to visually illustrate the size-dependent trends. **B)** The value by which the PL maximum shifts after exposure to various atmospheres compared to its initial PL maximum is plotted for several different sized fractions. Dashed lines are shown to visually illustrate the size-dependent trends. In figure A) and B), where error bars are not visible, the associated error value falls within the range of the symbol size.

Dry O₂
- Energy (*E*) transfer from ncSi:AB to O₂ excites it to the singlet state (*) (photosensitization)
- Excited O₂ reacts at the ncSi:AB surface resulting in irreversible surface oxidation

Wet Ar
H₂O adsorbs to the ncSi:AB surface and passivates surface defects and dangling bonds

Wet O₂
- H₂O adsorbs to the ncSi:AB surface passivating defects and preventing O₂ from approaching
- H₂O adsorbed near surface silanol groups helps promote the reaction of O₂ at the ncSi:AB surface resulting in irreversible surface oxidation

Dry Ar
No interaction, but minimal oxidation occurs in presence of residual air

Scheme 1. Summary of proposed interactions occurring at the ncSi:AB surface under each atmosphere.

Continuous AQY curves and PL spectra (similar to those described above for fraction 16) were measured for film samples of four different sized fractions (11, 13, 16, and 18). The difference in PL AQY value (AQY final – AQY initial) for each fraction exposed to each atmosphere is plotted in **Figure 4A**. Similar results as previously outlined for fraction 16 are observed for all sizes examined, where the decrease in AQY is greatest for samples exposed to dry O_2, followed by wet O_2, then dry Ar, and samples exposed to wet Ar show an increase in AQY. Size-dependent trends can also be extracted from these results, where the AQY shift increases in magnitude as the particle size increases for films exposed to dry Ar, dry O_2, and wet O_2. Work examining photosensitization of porous silicon suggests that larger particles show the greatest PL degradation due to their larger surface region, which would increase the probability of O_2 interacting at the surface.[14c] Despite the presence of ligands at the ncSi surface this effect may also occur in our case, such that more PL quenching is possible for the largest particles. This trend may also be explained by the fact that quenching by photosensitization is most efficient when the PL energy occurs at 1.63 eV (760nm).[14b] The PL spectra of all fractions have some intensity at this energy but as the particle size decreases the PL maximum blue shifts away from this value so the smaller particles have less overlap with this photosensitization wavelength compared to the largest particles.

In the case where the films are exposed to wet Ar, the magnitude of the AQY increase, increases with increasing size. This trend may also be explained by larger particles having larger surfaces, which likely result in a higher number of surface defects with which H₂O is able to interact and passivate.

The PL blue shift (final PL maximum – initial PL maximum) in eV for fractions exposed to all atmospheres

(**Figure 4B**), shows a size-dependent trend in which a larger PL blue shift is observed for larger particles for all conditions except wet Ar. Since blue shifting of ncSi emission energy has been attributed to shrinking of the nanocrystalline core due to the formation of an oxide layer for ncSi exposed to air overtime,[12] it makes sense that the larger particles have the ability to blue shift more than the smaller particles, which contain less core Si. Additionally, it has been reported that particles that have less initial surface oxidation show greater PL blue shifting upon further oxidation,[27] which fits with the FTIR (**Figure 1A**) and XPS (**SI Figure 3A**) measurements of pristine ncSi:AB presented here. XPS measurements of size-separated ncSi:AB after exposure to air overtime also indicate that the atomic % of oxygen is greatest for larger particles (**SI Figure 3B**), which is consistent with the observed size-dependent PL blue shifting trends. The PL shift magnitude and slope of each trend follows the order where wet O_2 > dry O_2 > dry Ar, which is consistent with the results previously explained for fraction 16, where the presence of H₂O with O_2 helps promote the irreversible oxidation of the ncSi:AB surface. Under exposure to wet Ar, the interaction of ncSi:AB with H₂O has a significant effect on the PL maximum, resulting in a shift of about 0.015eV for all sizes. While PL shifting is likely to occur from surface oxidation from residual air in the system, the lack of size-dependence observed for wet Ar on the PL maximum of ncSi:AB indicates that there may be size-independent surface effects that are responsible for PL blue shift observed. More extensive study, however, is required to confirm and identify the effects responsible for the observations in wet Ar.

In this study, we have shown that by quantitatively monitoring the effects O_2, H₂O and O_2-H₂O environments have on the PL wavelength, intensity and absolute

quantum yield of ncSi:AB one can obtain valuable insight into the effect of the size of the silicon core on their chemical reactivity. With the collected results of this investigation it behooves one to think about the molecules and materials effects that most likely contribute to the trends observed for the size-dependent reactivity of ncSi:AB with O_2, H_2O and O_2-H_2O.

It is clear from the results presented in this paper that both O_2 and H_2O and mixtures thereof can oxidize the silicon core of ncSi:AB. The contributing effects include size-dependent steric effects relating to the curvature of the silicon core and its effect on packing of covalently bound surface allylbenzene groups, and quantum size effects of the silicon core and how these affect valence and conduction band energies and gaps. The smaller the silicon core with its larger electronic band gap and higher ionization potential, the harder it would be to oxidize with O_2, H_2O and O_2-H_2O. Additional factors include the surface area of each particle, which relates to the number of surface defects present per ncSi:AB and the number of H_2O or O_2 species that can interact with each particle, as well as the size of the ncSi:AB core, which limits the extent of possible oxidation. Within the framework of this simple model, the surface area, core size and electronic factors favor increased chemical reactivity as the size of ncSi:AB increases.

Conclusions

In this chemical reactivity study, the effect of O_2, H_2O, and a combination of both on the PL and AQY of relatively monodisperse ncSi:AB have been investigated for a range of particle sizes. The dominant interactions thought to be occurring at the ncSi:AB surface under each atmosphere are collected together in **Scheme 1**. To amplify, we have shown that O_2 alone is capable of quenching and blue shifting PL, and that PL quenching likely occurs from a combination of reversible photosensitization and irreversible surface oxidation. In the presence of H_2O, the PL quenching that occurs from O_2 is minimized, and PL blue shifting is increased, likely due to the passivation of surface defects and dangling bonds by H_2O to create Si-OH species that help promote further irreversible surface oxidation by O_2 in the presence of H_2O. Exposure to H_2O alone results in an increase in the AQY. In all environments, the AQY changes observed increased with increasing particle size, and with the exception of exposure to wet Ar, the PL shifts observed increased with increasing size. Furthermore, in this work we have also shown that the chemical reactivity of the ncSi:AB surface with H_2O and/or O_2 is increased under continuous illumination with UV light.

ASSOCIATED CONTENT

Supporting Information. Scanning transmission electron microscopy images and XPS data are available in the Supporting Information. This material is available free of charge via the Internet at http://pubs.acs.org.

AUTHOR INFORMATION

Corresponding Author

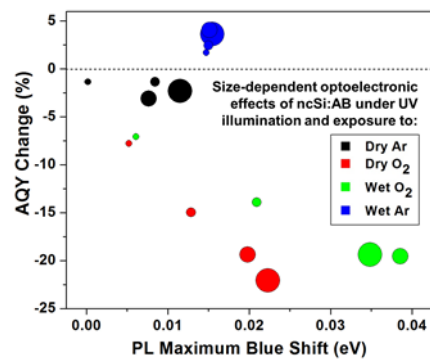* E-mail: gozin@chem.utoronto.ca

REFERENCES

(1) Canham, L. T. *Appl. Phys. Lett.* **1990**, *57*, 1046.

(2) (a) Mastronardi, M. L.; Maier-Flaig, F.; Faulkner, D.; Henderson, E. J.; Kübel, C.; Lemmer, U.; Ozin, G. A. *Nano Lett.* **2012**, *12*, 337. (b) Mastronardi, M. L. M.; Hennrich, F.; Henderson, E. J.; Maier-Flaig, F.; Blum, C.; Reichenbach, J.; Lemmer, U.; Kübel, C.; Wang, D.; Kappes, M. M.; Ozin, G. A. *J. Am. Chem. Soc.* **2011**, *133*, 11928. (c) Hessel, C. M.; Reid, D.; Panthani, M. G.; Rasch, M. R.; Goodfellow, B. W.; Wei, J.; Fujii, H.; Akhavan, V.; Korgel, B. A. *Chem. Mater.* **2012**, *24*, 393.

(3) Ledoux, G.; Guillois, O.; Porterat, D.; Reynaud, C.; Huisken, F.; Kohn, B.; Paillard, V. *Phys. Rev. B* **2000**, *62*, 15942.

(4) (a) Miller, J. B.; Van Sickle, A. R.; Anthony, R. J.; Kroll, D. M.; Kortshagen, U. R.; Hobbie, E. K. *ACS Nano* **2012**, *6*, 7389. (b) Rinck, J.; Schray, D.; Kübel, C.; Powell, A. K.; Ozin, G. A. *Small* **2014**, 1.

(5) (a) Wu, C.; Bull, B.; Szymanski, C.; Christensen, K.; McNeill, J. *ACS Nano* **2008**, *2*, 2415. (b) Henderson, E. J.; Shuhendler, A. J.; Prasad, P.; Baumann, V.; Maier-Flaig, F.; Faulkner, D. O.; Lemmer, U.; Wu, X. Y.; Ozin, G. A. *Small* **2011**, *7*, 2507. (c) Mastronardi, M. L.; Henderson, E. J.; Puzzo, D. P.; Chang, Y.; Wang, Z. Bin; Helander, M. G.; Jeong, J.; Kherani, N. P.; Lu, Z.; Ozin, G. A. *Small* **2012**, *8*, 3647. (d) Cheng, K.-Y.; Anthony, R.; Kortshagen, U. R.; Holmes, R. J. *Nano Lett.* **2011**, *11*, 1952. (e) Cheng, K.-Y.; Anthony, R.; Kortshagen, U. R.; Holmes, R. J. *Nano Lett.* **2010**, *10*, 1154.

(6) Liu, S.-M.; Sato, S.; Kimura, K. *Chem. Mater.* **2006**, *18*, 637.

(7) Pi, X. D.; Liptak, R. W.; Deneen Nowak, J.; Wells, N. P.; Carter, C. B.; Campbell, S. A; Kortshagen, U. *Nanotechnology* **2008**, *19*, 245603.

(8) Zou, J.; Sanelle, P.; Pettigrew, K. A.; Kauzlarich, S. M. *J. Clust. Sci.* **2006**, *17*, 565.

(9) (a) Buriak, J. *Chem. Mater.* **2013**, *26*, 763. (b) Kelly, J. A; Shukaliak, A. M.; Fleischauer, M. D.; Veinot, J. G. C. *J. Am. Chem. Soc.* **2011**, *133*, 9564. (c) Kelly, J. A; Veinot, J. G. C. *ACS Nano* **2010**, *4*, 4645.

(10) Pi, X.; Wang, R.; Yang, D. *J. Mater. Sci. Technol.* **2014**, *30*, 639.

(11) Jurbergs, D.; Rogojina, E.; Mangolini, L.; Kortshagen, U. *Appl. Phys. Lett.* **2006**, *88*, 233116.

(12) Anthony, R.; Kortshagen, U. *Phys. Rev. B* **2009**, *80*, 115407.

(13) (a) Pereira, R. N.; Rowe, D. J.; Anthony, R. J.; Kortshagen, U. *Phys. Rev. B* **2011**, *83*, 155327. (b) Delley, B.; Steigmeier, E. *Phys. Rev. B* **1993**, *47*, 1397.

(14) (a) Konstantinova, E. A.; Demin, V. A.; Vorontzov, A. S.; Ryabchikov, Y. V.; Belogorokhov, I. A.; Osminkina, L. A.; Forsh, P. A.; Kashkarov, P. K.; Timoshenko, V. Y. *J. Non. Cryst. Solids* **2006**, *352*, 1156. (b) Kovalev, D.; Gross, E.; Künzner, N.; Koch, F.; Timoshenko, V.; Fujii, M. *Phys. Rev. Lett.* **2002**, *89*, 137401. (c) Kovalev, D.; Gross, E.; Diener, J.; Timoshenko, V. Y.; Fujii, M. *Appl. Phys. Lett.* **2004**, *85*, 3590.

(15) (a) Miura, T.; Niwano, M.; Shoji, D.; Miyamoto, N. *J. Appl. Phys.* **1996**, *79*, 4373. (b) Niwano, M.; Kageyama, J.; Kurita, K. *J. Appl. Phys.* **1994**, *76*, 2157.

(16) (a) Švrček, V.; Sasaki, T.; Shimizu, Y.; Koshizaki, N. *Appl. Phys. Lett.* **2006**, *89*, 213113. (b) Li, S.; Silvers, S. J.; El-shall, M. S.; Commonwealth, V.; Uni, V. **2006**, *5647*, 1794.

(17) Stewart, M. P.; Buriak, J. M. *J. Am. Chem. Soc.* **2001**, *123*, 7821.

(18) Panthani, M.; Hessel, C.; Reid, D.; Casillas, G.; Jose-Yacaman, M.; Korgel, B. A. *J. Phys. Chem. C* **2012**, *116*, 22463.

(19) Mangolini, L.; Jurbergs, D.; Rogojina, E.; Kortshagen, U. *J. Lumin.* **2006**, *121*, 327.

(20) Faulkner, D. O.; McDowell, J. J.; Price, A. J.; Perovic, D. D.; Kherani, N. P.; Ozin, G. A. *Laser Photon. Rev.* **2012**, *6*, 802.

(21) Lopinski, G.; Wayner, D. *Mater. Matters* **2008**, *3*, 38.

(22) Bullen, C.; Mulvaney, P. *Langmuir* **2006**, *22*, 3007.

(23) Hessel, C. M.; Rasch, M. R.; Hueso, J. L.; Goodfellow, B. W.; Akhavan, V. A; Puvanakrishnan, P.; Tunnel, J. W.; Korgel, B. A. *Small* **2010**, *6*, 2026.

(24) Mei, B. C.; Oh, E.; Susumu, K.; Farrell, D.; Mountziaris, T. J.; Mattoussi, H. *Langmuir* **2009**, *25*, 10604.

(25) (a) Lockwood, R.; Hryciw, A.; Meldrum, A. *Appl. Phys. Lett.* **2006**, *89*, 263112. (b) Priolo, F.; Franzò, G.; Pacifici, D.; Vinciguerra, V.; Iacona, F.; Irrera, A. *J. Appl. Phys.* **2001**, *89*, 264.

(26) Yang, J.; Liptak, R.; Rowe, D.; Wu, J.; Casey, J.; Witker, D.; Campbell, S. A.; Kortshagen, U. *Appl. Surf. Sci.* **2014**.

(27) Froner, E.; Adamo, R.; Gaburro, Z.; Margesin, B.; Pavesi, L.; Rigo, A.; Scarpa, M. *J. Nanoparticle Res.* **2006**, *8*, 1071.

SYNOPSIS TOC:

Size-dependent optoelectronic effects of ncSi:AB under UV illumination and exposure to:
- Dry Ar
- Dry O$_2$
- Wet O$_2$
- Wet Ar

Supporting Information:

# Size-Dependant Chemical Reactivity of Silicon Nanocrystals

Melanie L. Mastronardi,[†] Kenneth K. Chen,[†] Kristine Liao,[†] Gilberto Casillas,[α] Geoffrey A. Ozin[†]*

[†]Department of Chemistry, University of Toronto, 80 St. George Street, Toronto, Ontario, Canada, M5S 3H6

[α]UOW Electron Microscopy Centre, University of Wollongong, New South Wales 2500, Australia

* To whom correspondence should be addressed: gozin@chem.utoronto.ca
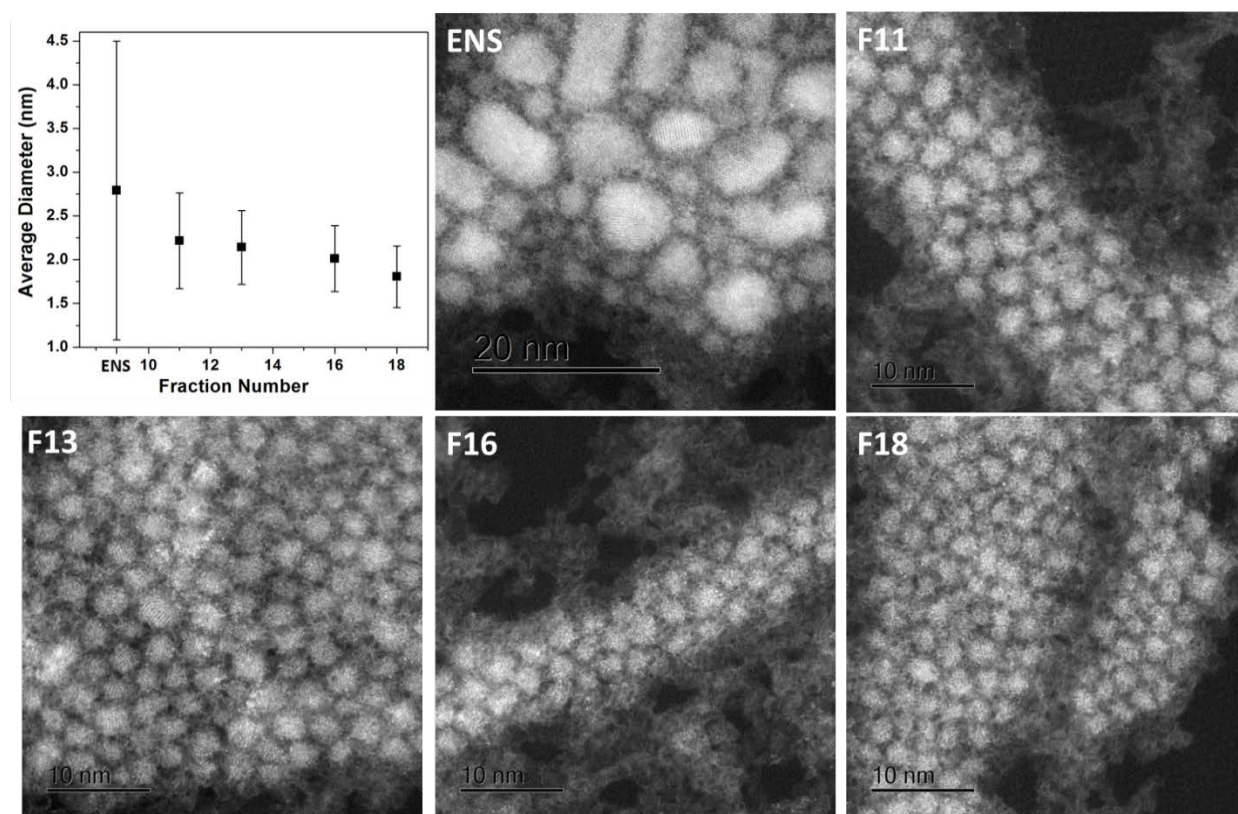
SI Figure 1. Middle Angle Annular Dark Field Scanning Transmission Electron Microscopy. Representative images of the polydisperse ensemble and select size-separated ncSi:AB fractions.
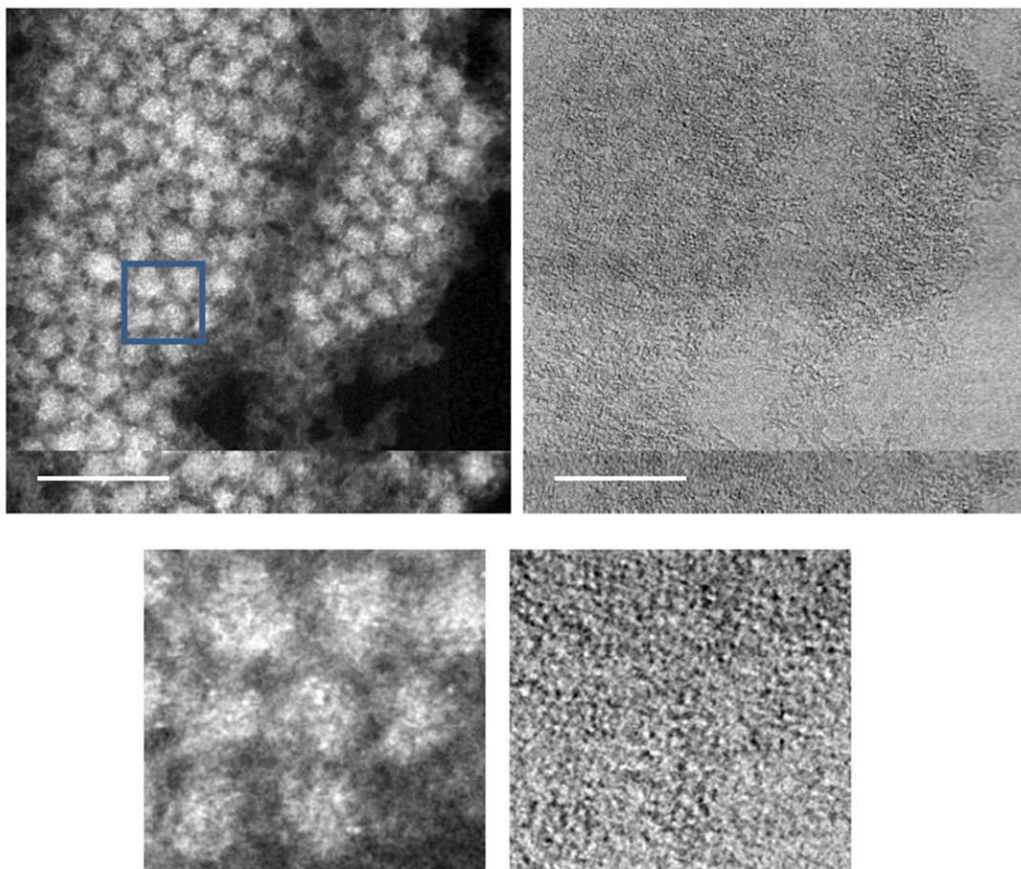
SI Figure 2. Scanning Transmission Electron Microscopy of Fraction 18. Top images show the same area measured under middle angle annular dark field (left) and bright field (right). Bottom images are a magnification of the area denoted by the blue square. Scale bar indicates 10 nm.
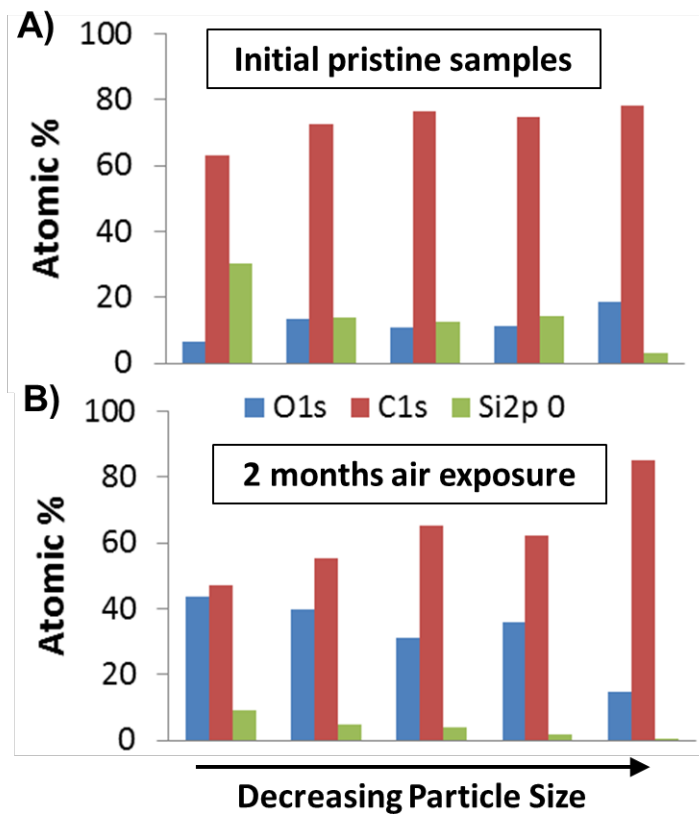
SI Figure 3. Atomic percent from X-ray photoelectron spectroscopy (XPS) of size-separated ncSi:AB. Atomic % of O1s, C1s and Si2p^0 species as determined by XPS for size-separated ncSi:AB of varying size immediately after synthesis (**A**), and after exposure to air for about 2 months (**B**).

SI Figure 4. Summary of proposed interactions occurring at the ncSi:AB surface under each atmosphere.